ICE STATION 2003 IN LAKE PÄÄJÄRVI, FINLAND

C. Wang[1], M. Leppäranta[1], K. Shirasawa[2], O. Huttunen[1], M. Ishikawa[2] and T. Takatsuka[2]

ABSTRACT
An automatic floating ice station was used in Lake Pääjärvi, Lammi in winter 2003 for monitoring the evolution of the ice conditions. The instrumentation included atmospheric, ice, and water sensors: temperature, humidity, wind speed and solar radiation for air; temperature and PAR (Photosynthetically Active Radiation) for ice; and temperature and currents for water. The station was deployed on the 15th of December 2002, and it was active for ice sensors until April 3 and for water and air sensors well beyond the final melting of the ice. At the time of the deployment the ice sheet was 25 cm thick, clear congelation ice, and it grew to the local record thickness of 80 cm during the winter. The station is the first of its kind, full air-ice-water recording system, used in Finnish lakes. The data and results are given in this presentation, concerning the ice heat budget and the transfer of solar radiation through the ice.

INTRODUCTION
Lake Pääjärvi (Fig. 1) is located in southern Finland with a maximum depth of 87m. Its mean depth is 14.4m and surface area is 13.4km^2. The lake is covered by ice every winter, with a mean period of about five months from mid December to early May of the next year. The

Fig.1. Lake Pääjärvi

annual mean maximum ice thickness is 55cm (Käarkäs, E., 2000).
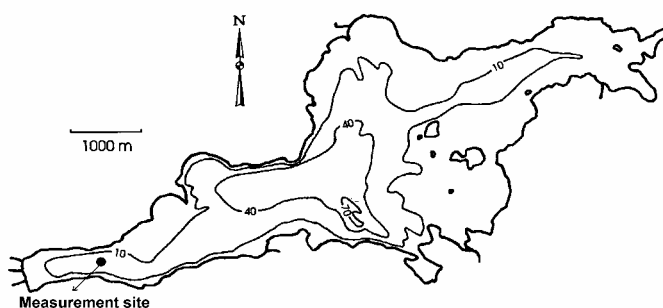
For monitoring the ice conditions, an automatic ice station was employed in winter 2002/2003, as shown in Fig. 1. The instrumentation included atmospheric, ice, and wa-

---

[1] Division of Geophysics, University of Helsinki, Finland.
[2] Institute of Low Temperature Science, Hokkaido University, Hokkaido, Japan.

ter sensors: temperature, humidity, wind speed and solar radiation for air; temperature and PAR (Photosynthetically Active Radiation) for ice; and temperature air-water-ice. In this paper, we first introduce the ice station. Then based on the recorded data, we give some analysis results about the heat budget on the air-ice surface and about the transfer of solar radiation through the ice.

ICE STATATION

The ice station consisted of three parts: a platform station, a thermistor string, and a current meter with CT sensor, located separately within about 150m. The platform was deployed on 15 December 2002, at 61°03′2.3″N and 25°03′48.2″E. It continuously made the measurements until 3 April 2003. As shown in Fig. 2a, this station was composed of a base, a mast with atmospheric instruments, and a thermistor measuring the ice and water temperature. The base was a board of 2m×2m balanced by four big stones in the water. The atmospheric instruments on the mast included three thermometers and two anemometers at two different heights, one hygrometer and one solar radiometer. The vertical positioning of these instruments is shown in Table 1.
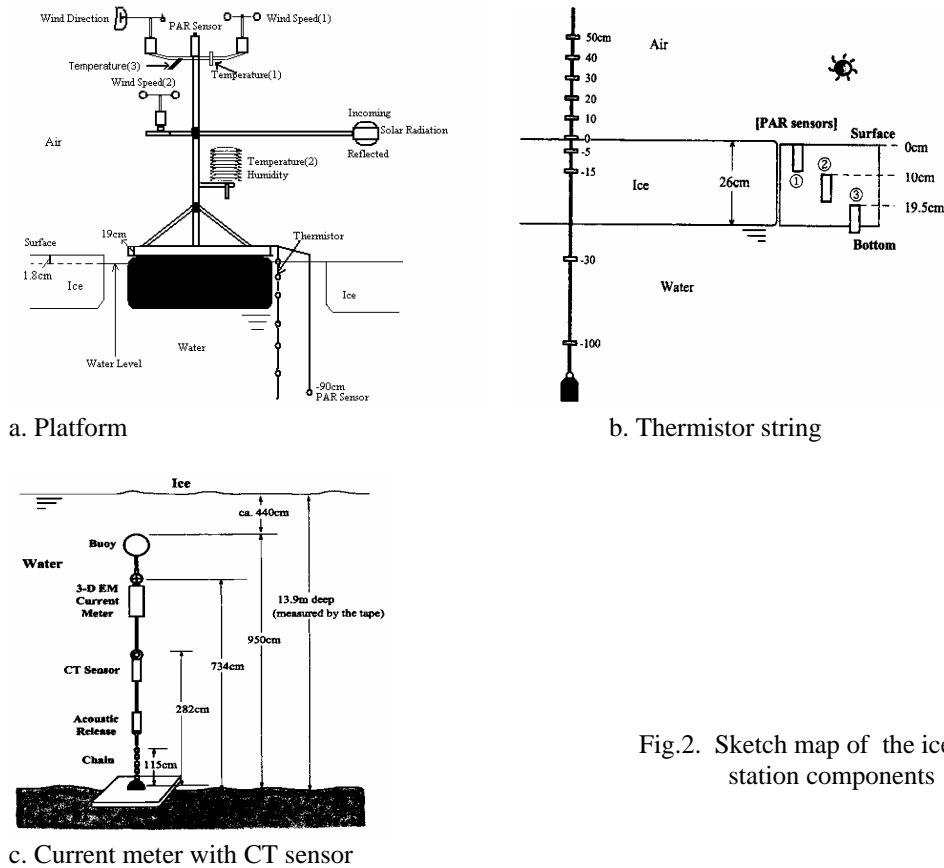

a. Platform

b. Thermistor string

c. Current meter with CT sensor

Fig.2. Sketch map of the ice
station components

The thermistor string was deployed at the site of 61°02′58.9″N and 25°03′50.3″E on 18 December 2002, and working till 3 April 2003. It was composed of ten thermistors for full air-ice-water temperature and PAR sensors (named 1[#]) for ice radiation, as shown in Fig. 2b. Another group of PAR sensors (named 2[#]), about half meter away from the PAR sensors at site 1[#], was deployed on 18 March 2002, and continuously working till 2 April 2003. The current meter with CT sensor was deployed at the site of

61°02′56.5″N and 25°03′49.9″E. They were anchored at the bottom of the lake with a chain 115cm long. The current speed, current direction, salinity and water temperature were measured from 18 December 2002 until 7 May 2003. The vertical position of the instruments in these two parts is also shown in Table 1. The sample rate of the instruments for the ice station is also shown in Table 1. The current and salinity were recorded every 30 minutes, and the PAR radiation was every 10 minutes, the other variables were recorded every 1 hour.

RESULTS AND DISCUSSION

During the time of deploying the station, the ice was clear congelation ice of 25cm thickness. It was 78cm on 26 Feb. 2003, and the highest thickness was 80cm during the winter. Temperature, heat budget and the transfer of solar radiation through the ice are parameters for ice growth and decay. In this section, they are analyzed with the recorded data.

Table 1. The sensors and their positions of the ice station

Ice station	Sensors	Height [*](cm)	Sample rate	Start time (UTC)
Platform	Wind Speed (1) Wind Direction Wind Speed (2)	215 215 120	1 hour	17.12.2002, 14:00

	Solar Radiation
	  Incoming
	  Reflected
		
		119
		110		

	Air temperature(1) Air temperature(2) Temperature(3) Humidity	197 95 197 95		
	Thermistor[**]	0, -10, -20, -40,-60, -80		

	PAR[**]
	  In the air [No. 3464]
	  In the water [No. 3434]
		
		200
		-90		

Thermistor String	PAR[**] in the ice(1[#])	0,-10,-19.5	10 min.	18.12.2002, 10:00
	PAR[**] in the ice(2[#]) (not shown in the figure)	0,-10,-30,-60		18.03.2003, 14:16
	Thermsitor (Logger SQ 1206)	50,40,30,20,10,0, -5,-15,-30,-100	1 hour	18.12.2002, 10:00

Current Meter with CT Sensor	ALEC ACM32M[***]
	  Current speed
	  Current Direction
	  North-south Component
	  East-west Component
	  Vertical Component
		
		734cm
		734cm
		734cm
		734cm
		734cm
			30 min	17.12.2002, 14:00

	ALEC MDS-CT[***]
	  Twater
	  Salinity
	  SigmaT
		
		282cm
		282cm
		282cm		

Note: [*] Height from the platform surface; [**] Depth from the water level;

[***] Height from the bottom of the lake.

The ice/water temperature

The ice/water temperature was measured at depth 0cm, 10cm, 20cm, 40cm, 60cm and 80cm at the platform, while it was measured at depth 0cm, 5cm, 15cm, 30cm and 100cm at the thermistor string (See Fig. 2 and Table 1). Fig. 3 shows the time series of vertical ice/water temperature measured at the platform and thermistor string. In general, the temperatures from the two sites are of similar variation characteristics, lower at the surface and increasing downward. The temperatures were lowest during the late December and early January, and late January and early February. However, there is significant difference. The temperatures at the thermistor string were lower than those at platform at the same depth when they were below zero degree. For example, the minimum surface temperature was –20.5°C at the thermistor string while –11.8°C at the platform on 7 January. For another example, in January, the 0°C isotherm at the platform, as shown in Fig.3a, was just downward to about –50 cm, while that at the thermistor string reached –98 cm (Fig.3b). The big difference implies that the platform itself may play an important role in the heat budget of the underneath water and ice, especially when the water is freezing. This effect must be taken into account in the future to avoid the systematic deviations.
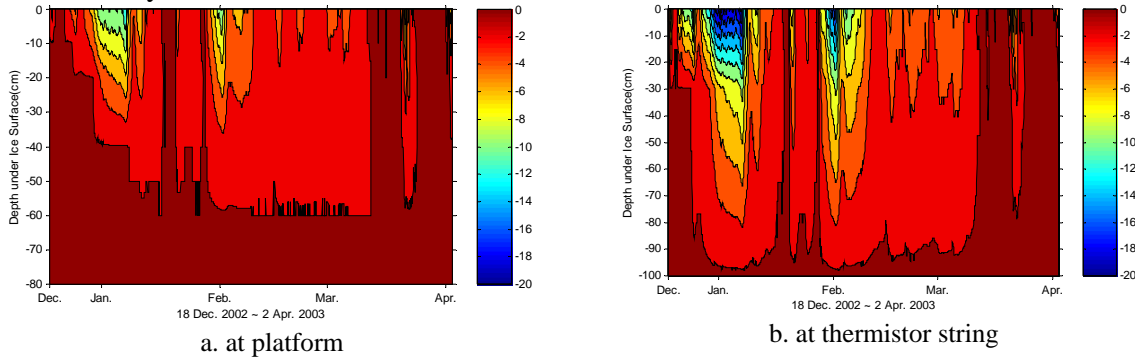

a. at platform   b. at thermistor string

Fig. 3. Time series of ice/water temperature

Heat budget of the ice

The heat exchange between ice and the atmosphere, including sensible heat flux, latent heat flux, solar radiation and long-wave radiation, controls the growth and decay of the ice. Here the results in January and March are shown.

<u>Sensible heat flux (Q_h) and latent heat flux (Q_e)</u>

Sensible and latent heat fluxes describe the turbulent heat exchange between the ice surface and the atmospheric boundary layer. They can be expressed with the bulk aerodynamic formula as follows,

$$Q_h = \rho_a c_a C_h (T_a - T_0)U \tag{1}$$

$$Q_e = \rho_a L_e C_e (q_a - q_0)U \tag{2}$$

where ρ_a and c_a are the density and specific heat of the atmosphere; C_h and C_e are the heat transfer coefficient for the sensible and latent heat respectively, generally related to the stratification of the atmosphere. They are often simply taken as constants ranging from 1.2×10^{-3}-1.75×10^{-3}, here both taken 1.32×10^{-3} [2]. L_e is the enthalpy of evaporation. T_0 and q_0 are the surface temperature and specific humidity. T_a, q_a and U are the air temperature, specific humidity and velocity at a reference height, here taking 1.97m above the platform surface, U is calculated from the measured wind velocity at the height of 215cm and 120cm assuming a logarithm wind profile. The specific humidity

51

is calculated with the formula $q = 0.622 E_{sat}(T)r/p$, where r is the relative humidity, $E_{sat}(T)$ is the saturate vapor pressure obtained by the *Magnus* formula.

As shown in Eq. (1), sensible heat flux relies on the wind speed and the temperature difference between the air and ice surface. The negative value means heat release from the ice to the air and vice versa. In January (Fig. 4a), the sensible heat fluxes were negative in early time and then fluctuated between positive and negative. There were some peaks because of the relatively large temperature difference between the air and ice surface and high wind speed. The magnitude generally ranged within –20 - +20 Wm^{-2}, with a mean value about –3.2Wm^{-2} in this month. In March (Fig. 4b), most of the sensible heat fluxes were positive, their range were mostly within –10 - 50Wm^{-2}, with a mean value about 6.8Wm^{-2}. The maximum value was 85Wm^{-2} and the minimum –14.4Wm^{-2}. The sensible heat fluxes were larger than those in January because of the higher temperature. As for the latent heat fluxes, in January they basically showed a similar pattern to the sensible heat flux (Figs. 4a and 4c), only with the amplitude down to about a half of it. While in March, they exhibited considerable difference from the sensible heat flux (Figs. 4b and 4d). Most of the values were negative. Positive latent heat flux in Figs. 4c and 4d indicated, according to Eq. (2), a higher specific humidity in the air than that of the ice surface. This is, however, very rarely happened.
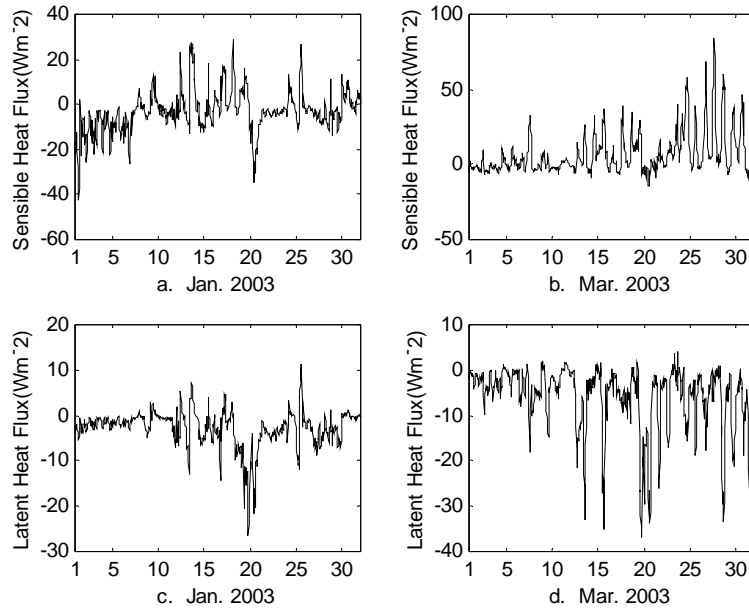

Fig. 4. Sensible heat flux(a and b) and Latent heat flux(c and d) in January and March

The net solar radiation flux (Q_{sn})
The net solar radiation was calculated from

$$Q_{sn} = Q_{si} - Q_{so}, \tag{3}$$

where Q_{si} and Q_{so} are the incoming and reflected solar radiation respectively. Here both are directly measured.

Taking account into the effect of the atmospheric turbidity and clouds, incoming solar radiation (Q_{si}) can be expressed as (Reed, 1977),

$$Q_{si} = S_0 \cdot E \cdot \sin^2(h) \cdot TR \cdot (1 - 0.62N + 0.0019\alpha), \qquad (4)$$

where S_0 is the solar constant, E is the eccentricity of Earth's orbit around Sun, h is the solar altitude, TR is the atmospheric turbidity, here taking 0.95 [3], α is noon solar altitude, N is cloud amount in tenths. The incoming solar radiation was measured directly and can be used to estimate the cloud cover with Eq.(4), and used for calculating long-wave radiation below.

As shown in Figs. 5a and 5b, since there was no solar radiation during the nocturnal time, the net solar radiation was zero. There is a striking phenomenon that some values of the net solar radiation appeared negative in January and before the middle of March. The possible reason would be: (1) the surface of the incoming solar radiation sensor was covered by snow/snow ice crystal, which reflected part of the incoming solar radiation back into the atmosphere and reduced the incoming solar radiation; (2) the irregular snow surface happened to form a paraboloid facing the sensor, which increased the received reflected radiation. This phenomenon disappeared after the snow began to melt in late March. In January and before the middle of March, the net solar radiation was very small, only tens of Wm^{-2}. After that, its order increased to hundreds of Wm^{-2}.
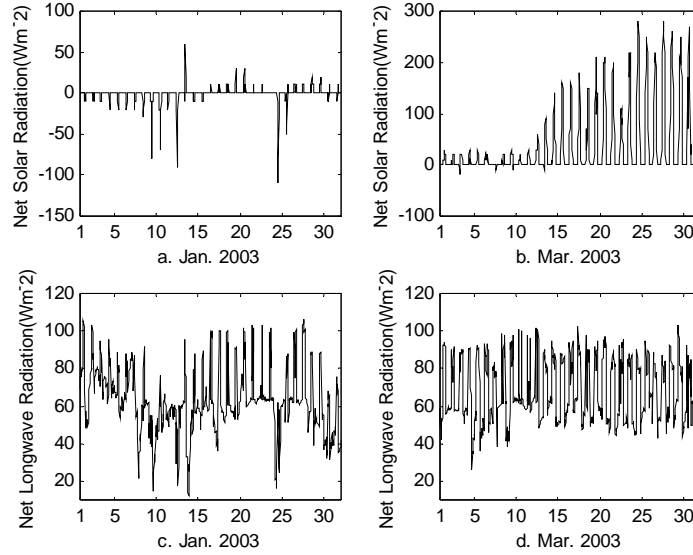

Fig. 5. Net solar radiation flux (a and b) and Net long-wave radiation flux(c and d) in January and March

The net long-wave radiation flux (Q_{ln})
The net long-wave radiation is due to the difference of the atmospheric and ice/snow surface radiation. It is expressed as,

$$Q_l = \varepsilon\sigma(T^4 - T_a^4(0.68 + 0.0036\sqrt{e})(1 + 0.18 \cdot N^2)), \qquad (5)$$

where ε is the water or ice/snow emissivity, equal to 0.99 for water and 0.97 for snow/ice, σ is Stefan Bolzman's constant, e is the water vapour pressure, N is cloud amount in tenths obtained from Eq. (4) above.

During the measurement period, the mean difference between clear-sky (N=0) and overcast sky (N=1) was $34 Wm^{-2}$ for net long-wave radiation. As shown in Figs. 5a and 5c, the net long-wave radiation was larger than that of net solar radiation in January.

The value was mainly within 20~100Wm^{-2}. In March (Fig. 5d), the net long wave radiation was mostly between 50-90 Wm^{-2}. Its variation was relatively stable compared with that in January. Compared with the net solar radiation in March, the magnitude of net long-wave radiation is much smaller after middle March.

Solar radiation in the ice and the extinction coefficient of the ice
When solar radiation transfers in the ice, it is extinguished by the ice. Its decay obeys the Beer's Law. After integrated within the range of wavelength 400-700nm (the range of PAR), we get,

$$I(z) = I_0 \exp(-\int_0^z k(z)\,dz) ,\qquad (6)$$

where $I(z)$ and I_0 denote the integrated radiation at depth z and net radiation into the ice surface. k is the integrated extinction coefficient with spectrum. Taking k_z as the extinction coefficient averaged over depth, it can be estimated as follows from Eq. (6),

$$k_z = -\frac{1}{z_1 - z_2} \ln\left[\frac{I(z_2)}{I(z_1)}\right].\qquad (7)$$

The solar radiation in the ice was measured by PAR sensors at two sites 1$^{\#}$ and 2$^{\#}$. When deploying PAR sensors at site 2$^{\#}$ on March 18, the snow thickness was 46cm and the ice thickness was 75cm. The measurement positions refer to Table 1. The measured radiation is quantum irradiance (q), and its unit is $\mu mol\,m^{-2}s^{-1}$. For physical problem, irradiance (E (unit: Wm^{-2})) is more universal. According to Reinart et al.(1998), there is a relationship between them at different depth for clear or turbidity water bodies. Ice can be considered as clear water. Here the ratio for q/E is taken as 4.6$\mu mol\ s^{-1}W^{-1}$. Figure 6 shows the measured irradiance at 0cm and 10cm depth at the two sites. As shown in Fig. 6: (1) Most of the irradiance in the ice was zero in January at site 1$^{\#}$(Fig.6a) because no solar radiation transferred into the ice (Fig. 5a). (2) Except for the diurnal changes, the radiation in the ice also changed with season. Due to the snow cover and the small solar angle, the irradiance was small before the mid-March (about 10th). After that, it increased several multiples (Fig. 6a). (3) The irradiance at 0cm at 2$^{\#}$ was much larger than that at 1$^{\#}$. The mean value was 255.7Wm^{-2} at 2$^{\#}$, while it was 102.5 Wm^{-2} at 1$^{\#}$ at the same period. It is likely due to the snow thickness thicker at 1$^{\#}$ than at 2$^{\#}$ because of the different deploying time, and the radiation was extinguished much more rapidly in snow than in ice (Wadhms, 2000). (4) The difference between 0cm and 10cm at 2$^{\#}$ was bigger than that at 1$^{\#}$ because most of the radiation is extinguished by snow.
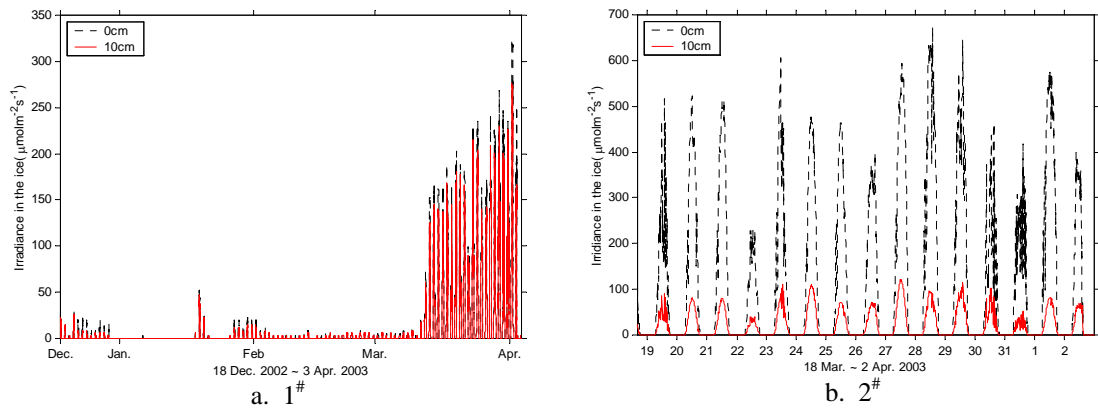

Fig.6.   Irradiance at 0cm (ice surface) and 10 cm of the ice (a. 1$^{\#}$; b. 2$^{\#}$)

Table 2. The minimum and maximum of k_z
($1^{\#}$: 17 Dec. 2002 ~ 3 Apr. 2003; $2^{\#}$: 18 March ~ 3 Apr. 2003)

Depth	k_z(m^{-1})					
	$1^{\#}$			$2^{\#}$		
	Min.	Max.	Mean	Min.	Max.	Mean
0-10cm	-9.405	19.775	1.647(1.329*)	-8.357	33.471	17.874
10-19.5cm	-17.001	11.499	0.966(0.876*)			
10-30cm				-2.850	3.890	1.6213
30-60cm				-1.758	1.066	-0.664

Note: * denotes the values from 18 March to 2 April 2003

The averaged extinction coefficient over depth was calculated with Eq. (7). Its range and mean values are shown in Table 2. The negative value means that scattering is dominant. The majority of the values were positive in the whole period. For comparison, Fig. 7 shows the calculated extinction coefficient k_z in the same period. In Fig. 7a, the extinction coefficient has no big difference at two depths on the whole, because most of the radiation is extinguished by snow. The mean extinction coefficients for the two depths of 0-10cm and 10-19.5cm are 1.647m^{-1} and 0.966m^{-1} respectively (see Table 2). While in Fig. 7b, the extinction at 0-10cm is much larger than that of 10-30cm and 30-60cm. Most radiation was extinguished by the uppermost 10cm and the mean value of extinction coefficient is 17.874 m^{-1} in the uppermost 10cm. Then it declines to 1.6213m^{-1} and -0.664 m^{-1} in the 10-30cm and 30-60cm respectively under the ice surface. In the 30-60 cm depth, the scattering function is dominant.
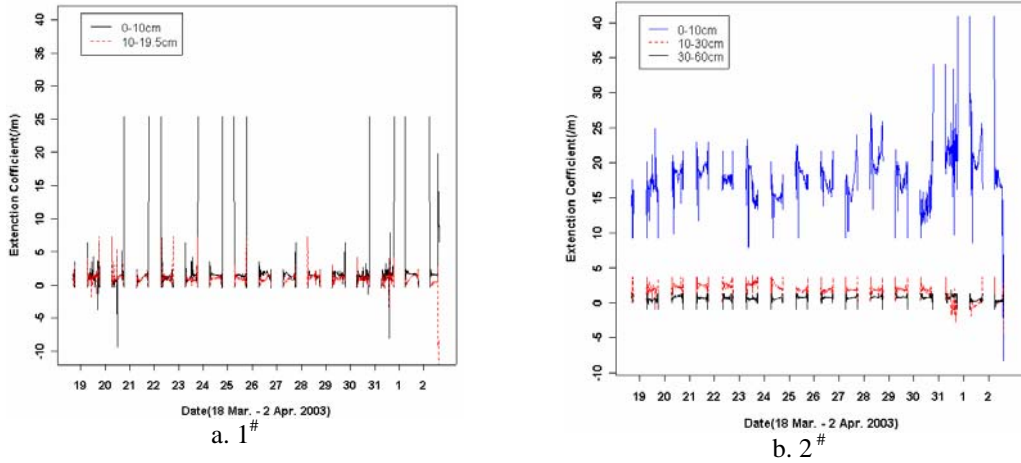

Fig. 7. the depth averaged k_z change with time during 18 March to 2 April 2003
(a. $1^{\#}$, b. $2^{\#}$)

CONCLUSION

We introduced our automatic ice station with full air-ice-water recording system in Lake Pääjärvi, Finland in winter 2002/2003. It is the first of its kind used in Finnish lakes. By comparing the two time series of ice/water temperature at the platform and at the thermistor string, we have found that the platform possibly played a big role concerning the heat budget and needs cautious consideration. The net long-wave radiation is relatively larger in January and early March, while the net solar radiation is relatively larger after mid-March. The net solar radiation shows some negative values in January and early March, the possible reasons were discussed above. The big difference of the radiation in

the ice was compared at the two sites measured by PAR sensors. The extinction coefficient in the uppermost 10cm is 1.647m^{-1} and 17.874m^{-1} at site 1[#] and 2[#] respectively.

REFERENCES

1. Kärkäs, E., 2000, The ice season of Lake Pääjärvi in southern Finland, *Geophysica*, 36(1-2), pp. 69-84.

2. Hapapala, J. and Leppäranta, M., 1996. Simulating the Baltic Sea ice season with a coupled ice-ocean model. *Tellus* 48A, pp. 622-643.

3. Omstedt, A., 1990. A coupled one-dimensional sea ice-ocean model applied to a semi-enclosed basin. *Tellus* 42 A, pp. 568-582.

4. Reed, R.K. 1977. An estimating insolation over the ocean, *J. Phys. Oceanogr*. 7, pp. 482-485.

5. Reinart, A., H. Arst, A. Blanco-Sequeiros and A. Herlevi, 1998. Relation between underwater irradiance and quantum irradiance in dependence on water transparency at differenct depths in the water bodies, *J. Geophys. Res*., 103, pp. 7749-7752

6. Wadhams, P., 2000. Ice in the ocean. Gordon and breach science publishers, pp. 86-88.